Numerical Stability of NonorthogonalFDTD Methods

Stephen D. Gedney, *Senior Member, IEEE,* and J. Alan Roden, *Member, IEEE*

***Abstract*—In this paper, a sufficient test for the numerical stability of generalized grid finite-difference time-domain (FDTD) schemes is presented. It is shown that the projection operators of such schemes must be symmetric positive definite. Without this property, such schemes can exhibit late-time instabilities. The origin and the characteristics of these late-time instabilities are also uncovered. Based on this study, nonorthogonal grid FDTD schemes (NFDTD) and the generalized Yee (GY) methods are proposed that are numerically stable in the late time for quadrilateral prism elements, allowing these methods to be extended to problems requiring very long-time simulations. The study of numerical stability that is presented is very general and can be applied to most solutions of Maxwell's equations based on explicit time-domain schemes.**

***Index Terms*—FDTD methods, numerical stability.**

I. Introduction

THE finite-difference time-domain (FDTD) method has been highly successful for the analysis of a plethora of electromagnetic interaction problems [1]. Yet one principal limitation of the classical FDTD method is the restriction to orthogonal grids. A number of techniques have been proposed to develop FDTD methods based on conformal meshing such as the contour path FDTD (CPFDTD) method [2], the nonorthogonal FDTD (NFDTD) method [3], and the discrete integral equation (DSI) [4] and generalized Yee (GY) methods [5]. The advantage of these techniques is that through the introduction of more generalized discretizations, error due to boundary discretization can be alleviated. Unfortunately, these and similar methods can sometimes suffer from late-time instabilities [6].

It was demonstrated by Craddock *et al.* that the source of instability of the CPFDTD method was due to the nonreciprocal nature of the original algorithm [7]. By analyzing the FDTD method as a passive circuit, an alternative stable and accurate solution was proposed. Such an extension is not directly applicable to the NFDTD, DSI, and GY methods because of the complexity of the projection operations required to project the fields normal to the grid faces onto the dual edges passing through the faces.

In this paper, it is demonstrated that the source of late-time instabilities in the NFDTD and DSI/GY methods is due to the basic definitions for the projection operators. Consequently, these methods can lead to formulations that are unstable in the late time *independent* of the time step. Alternative methods based on the NFDTD and the DSI/GY algorithms are proposed that are accurate and stable when employing quadrilateral prism elements (i.e., elements that are orthogonal in the vertical direction and irregular quadrilaterals in the horizontal direction).

Manuscript received March 25, 1998; revised November 15, 1999. This work was supported in part by the National Science Foundation under Grants ECS-9624628 and CDA-9502645 and the Army Research Office under Grant DAAH04-94-G-0243.

S. D. Gedney is with the Department of Electrical Engineering, University of Kentucky, Lexington, KY 40506-0046 USA.

J. A. Roden is with IBM Personal Systems Group, IBM Corporation, Research Triangle Park, NC 27709 USA.

Publisher Item Identifier S 0018-926X(00)01650-1.

II. General Formulation

The FDTD methods described herein assume a dual-staggered grid with an edge-based discretization of Maxwell's equations. Specifically, the electric field intensity is projected onto the edges of a *primary* grid and the magnetic field intensity is projected onto the edges of the *secondary* grid. Implementing Maxwell's curl equations in their integral form, the flux densities normal to the primary and secondary grid faces are naturally updated given the circulation of the dual field about the faces. Before performing the field update, the normal flux density vector must be projected onto the dual edge passing through the face. This is accomplished in the NFDTD algorithm [3] via the local Jacobian tensor and local interpolation and a local interpolation scheme in the DSI and GY methods [5], [8]. The details of these algorithms are not repeated here. Rather, the reader is referred to the original articles as well as [9] for a detailed summary of the algorithms.

Both the NFDTD and the DSI/GY methods result in explicit update schemes that can be expressed in general form as a coupled set of first-order difference equations

$$b^n = b^{n-1} - \Delta t C_e D_\epsilon A_d d^{n-(1/2)} \tag{1}$$

$$d^{n+(1/2)} = d^{n-(1/2)} + \Delta t C_h A_b b^n \tag{2}$$

where d and b are vectors of the discrete vector flux densities, the superscripts refer to discrete time, C_e and C_h represent the discrete contour integrals of the electric and magnetic fields about primary and secondary cell faces, respectfully, D_ϵ is a diagonal matrix with entries representing the inverse of the relative permittivity, and A_b and A_d are the projection matrices. Note that for simplicity the domain is assumed to be lossless and nonmagnetic. However, the following analyses are not limited by these simplifications.

III. Stability Analysis

The coupled difference equations in (1) and (2) are explicit in nature and are conditionally stable. To derive a sufficient stability condition, the coupled difference equations are reposed as a single first-order difference equation. To this end, first substitute (1) into (2). Then, introducing the vector

$$w^n = \begin{bmatrix} b^n \\ d^{n+(1/2)} \end{bmatrix} \tag{3}$$

(1) and (2) are reposed as a first-order difference equation

$$w^n = Gw^{n-1} \tag{4}$$

where

$$G = \begin{bmatrix} I & -\Delta t C_e D_\epsilon A_d \\ \Delta t C_h A_b & I - \Delta t^2 C_h A_b C_e D_\epsilon A_d \end{bmatrix}. \tag{5}$$

Let w^0 be the initial condition or the input into the system. Then, from (4)

$$w^n = G^n w^0 \tag{6}$$

where G^n represents G raised to the nth power. To ensure stability for a passive linear system $\lim_{n\to\infty} \|w^n\| \leq \|w^0\|$ must be satisfied. This is true if there exists a constant K, such that

$$\|G^n\|_2 \leq K(T) \qquad 0 \leq \Delta t < \tau, \quad 0 \leq n\Delta t \leq T \tag{7}$$

for all positive values of n, where the subscript 2 refers to the 2-norm, τ is a constant that is dependent on the spatial discretization and later defined in (18), and T is the duration. A necessary condition for (7) to be satisfied is that the eigenvalues of G must satisfy $|\lambda_G| \leq 1$ and G must have a complete set of distinct eigenvalues and eigenvectors (i.e., G is diagonalizable) [11].

The eigenspectrum of G is explored from the eigenvalue equation

$$Gw = \lambda_G w. \tag{8}$$

Subtracting the identity matrix from both sides of (8) leads to

$$(G - I)w = (\lambda_G - 1)w \rightarrow \tilde{G}w = \mu w \tag{9}$$

where $\lambda_G = 1 + \mu$. This is written more explicitly as

$$\begin{bmatrix} 0 & -\Delta t C_e D_\epsilon A_d \\ \Delta t C_h A_b & -\Delta t^2 C_h A_b C_e D_\epsilon A_d \end{bmatrix} \begin{bmatrix} w_1 \\ w_2 \end{bmatrix} = \mu \begin{bmatrix} w_1 \\ w_2 \end{bmatrix}. \tag{10}$$

The first row of (10) is multiplied by $\Delta t C_h A_b$, leading to

$$-\Delta t^2 \mu^{-1} C_h A_b C_e D_\epsilon A_d w_2 = \Delta t C_h A_b w_1. \tag{11}$$

Then, substituting (11) for the first term from the second row of (10), leads to

$$(\mu^2 + \mu \Delta t^2 M + \Delta t^2 M) w_2 = 0 \tag{12}$$

where

$$M = C_h A_b C_e D_\epsilon A_d \tag{13}$$

which represents the discrete curl–curl operation. At this point, it is assumed that M is diagonalizable. Then, introducing P, the matrix of eigenvectors of M and D_λ, the diagonal matrix containing the eigenvalues of M, M is diagonalized as

$$P^{-1} M P = D_\lambda. \tag{14}$$

Diagonalizing (12) leads to a quadratic characteristic equation

$$\mu^2 + \mu \Delta t^2 \lambda_m + \Delta t^2 \lambda_m = 0 \tag{15}$$

where λ_m are the eigenvalues of M. This leads to the relationship

$$\mu = \frac{-\Delta t^2 \lambda_m}{2} \pm \sqrt{\left(\frac{\Delta t^2 \lambda_m}{2}\right)^2 - 2\left(\frac{\Delta t^2 \lambda_m}{2}\right)}. \tag{16}$$

Finally, from (16), the eigenvalues for G are determined as

$$\lambda_G = 1 - \frac{\Delta t^2 \lambda_m}{2} \pm \sqrt{\left(\frac{\Delta t^2 \lambda_m}{2}\right)^2 - 2\left(\frac{\Delta t^2 \lambda_m}{2}\right)}. \tag{17}$$

Earlier, it was stated that a necessary condition for (7) is for $|\lambda_G| \leq 1$ and that the λ_G are distinct. Observing (17), this will be true if:

1) λ_m are positive real and distinct;
2) $(\Delta t^2 \lambda_m / 2) \leq 2$.

The second requirement leads to a restriction on the time step. Specifically, the time step is bound by τ, where from (7) and condition 2)

$$\tau = \frac{2}{\sup(\sqrt{\lambda_m})} = \frac{2}{\sup(\sqrt{(C_h A_b C_e D_\epsilon A_d)})}. \tag{18}$$

A similar bound was derived in [10]. (Note that the square root was neglected in [10].)

It is observed that if $\Delta t < \tau$ and λ_m is positive real, then the term within the radical in (17) will be negative. Thus, (17) can be rewritten as

$$\lambda_G = \left(1 - \frac{\Delta t^2 \lambda_m}{2}\right) \pm j\sqrt{2\left(\frac{\Delta t^2 \lambda_m}{2}\right) - \left(\frac{\Delta t^2 \lambda_m}{2}\right)^2}. \tag{19}$$

It is seen immediately that $|\lambda_G| = 1$ for all λ_m that are real and ≥ 0. Interestingly, this is expected since without dissipation, the total energy in the system is unchanged with time.

A complex λ_m will lead to an eigenpair of λ_G with one of the eigenvalues lying outside of the unit circle independent of Δt (including $\Delta t < \tau$). Subsequently, the system will be unconditionally unstable for all Δt. This instability will typically occur in late time and is characterized by a high-frequency oscillation with exponential growth. This is discussed further in the Appendix. It can further be shown that adding loss into the medium is not sufficient to push the eigenvalue into the unit circle. At best, it will push it closer to the unit circle, delaying the corruption of data into later time.

Based on this analysis, it is thus finally concluded that (1) and (2) will be stable iff 1) M is a positive definite matrix with distinct real eigenvalues and 2) $0 < \Delta t < \tau$, where τ is defined by (18).

A. Discussion

For the classical FDTD scheme the Courant limit alone is a sufficient condition for stability. This is strictly because $M = C_h C_e$ is positive definite. However, for general grid schemes such as the NFDTD and DSI/GY methods, the time stability limit is a necessary but not sufficient condition. M must also be positive definite.

As originally posed, the NFDTD and DSI/GY methods do not result in a positive definite M for general meshing. This is because the projection matrices A_b and A_d are nonsymmetric. Thus, these methods suffer from late-time instability. The question that remains is what are the necessary conditions for A_b and A_d to produce a stable scheme?

It is first noted that even for nonorthogonal grids, the product of the circulation matrices $C_h C_e$ is positive definite. It can also be shown that if A_d and A_b are positive definite symmetric, then $C_h A_b C_e A_d$ will be positive definite. Unfortunately, if ϵ_r is inhomogeneous, then $M = C_h A_b C_e D_\epsilon A_d$ may no longer be positive definite since $D_\epsilon A_d$ will be nonsymmetric. An effective way to force symmetry in the projection operator is to approximate (1) as

$$b^n = b^{n-1} - \Delta t C_e D_\epsilon^{1/2} A_d D_\epsilon^{1/2} d^{n-(1/2)}. \tag{20}$$

Then M is rewritten as

$$M \approx C_h A_b C_e D_\epsilon^{1/2} A_d D_\epsilon^{1/2}. \tag{21}$$

If A_d is symmetric positive definite, then $D_\epsilon^{1/2} A_d D_\epsilon^{1/2}$ will also be symmetric positive definite. Subsequently, M will be positive definite for inhomogeneous medium.

It must be realized that this is an approximation. The projection operation $e = D_\epsilon^{1/2} A_d D_\epsilon^{1/2} d$ maps the normal flux density to the field intensity projected on the edge passing through the face. Examining the ith entry of the vector e

$$e_i = a_{d_{i,i}} \frac{d_i}{\epsilon_{r_i}} + \sum_{j=1}^{M} a_{d_{i,j}} \frac{d_j}{\sqrt{\epsilon_{r_i}\epsilon_{r_j}}} \tag{22}$$

where $a_{d_{i,j}}$ is the entry of matrix A_d in the ith row and jth column. The diagonal term of the projection operation is unchanged. Whereas the off-diagonal terms are normalized by an effective permittivity expressed as the geometric mean of the permittivities of the two adjacent edges. It is demonstrated in Section V that this approximation does not significantly degrade the accuracy of the NFDTD or GY algorithms.

Finally, it is realized that if the projection operators can be posed as symmetric positive definite matrices, then the explicit scheme can be rendered stable within the time-stability limit.

IV. Symmetric Projection Operators

A. The NFDTD Algorithm

The NFDTD algorithm, as proposed by Lee *et al.* [3], is formulated through a discretization of Maxwell's curl equations in local curvilinear coordinates on an irregular structured dual grid. The curvilinear coordinates are chosen locally to each face of a primary or secondary grid cell. The flux normal to each cell face (or the contravariant field) is then calculated from the net circulation of the dual covariant field about the edges bounding the face using Ampere's or Faraday's laws. Once the normal fluxes are known, they must be projected onto the dual edge passing through the face in order to perform the update of the dual flux vector. The contravariant field vectors are then projected onto the covariant field vectors. The contravariant-to-covariant field projection is performed with the use of the metric tensor that is computed from the local curvilinear coordinates. Specifically

$$D_i = \sum_{j=1}^{3} g_{i,j} D^j \tag{23}$$

where D^j are the contravariant fields normal to the local grid faces, D_i is the covariant field passing through the ith face, and

$$g_{i,j} = \vec{A}_i \cdot \vec{A}_j \tag{24}$$

where $\vec{A}_i$ and $\vec{A}_j$ are the unitary vectors defined for the ith and jth coordinate axes.

To perform the projection as specified by (23) and (24), the fields weighted by the off-diagonal elements of the metric tensor are not uniquely known since only one flux vector is associated with each cell face. Subsequently, an averaging scheme is used to perform the update. Lee *et al.* [3] originally suggested using a simple linear average. Thus, the projection onto E_1 would be expressed as

$$\begin{aligned} D_1|_{i,j,k}^{n+(1/2)} = {} & g_{11} D^1|_{i,j,k}^{n+(1/2)} + \tfrac{1}{4} g_{12} (D^2|_{i,j,k}^{n+(1/2)} \\ & + D^2|_{i+1,j,k}^{n+(1/2)} + D^2|_{i,j-1,k}^{n+(1/2)} + D^2|_{i+1,j-1,k}^{n+(1/2)}) \\ & + \tfrac{1}{4} g_{13} (D^3|_{i,j,k}^{n+(1/2)} + D^3|_{i+1,j,k}^{n+(1/2)} + D^3|_{i,j,k-1}^{n+(1/2)} \\ & + D^3|_{i+1,j,k-1}^{n+(1/2)}) \end{aligned} \tag{25}$$

where the (i,j,k) are the discrete coordinates of the edge. It is noted that the entries of (25) would contribute to one row of A_d in (2).

The local metric tensor *assumes* a locally curvilinear coordinate system based on local cell face information. However, if the grid is irregular, then the off-diagonal terms of the metric tensor are not consistent between adjacent faces. This arises because the normal vectors of the adjacent faces may not all be colinear with the contravariant vector for that face. This results in asymmetry in A_d and A_b.

An alternative projection scheme was recently introduced by Roden [6]. This projection method will be referred to as the G^{sym} method. To this end, the assumption is made that the primary and dual grids are *locally* regular. Under this assumption, the dual and primary grids are *locally* equivalent. Subsequently, the projections for the primary and secondary grids may be defined *independently*. This leads to a simple unambiguous definition of the metric tensor g.

The covariant field components for the primary grid are computed by projecting each field component individually. These projections are accomplished entirely from primary grid edge vectors. Likewise, the covariant fields for the secondary grid are computed using only secondary grid edge vectors. Using this technique, the projection operation in (23) is compactly stated as

$$E_i = g_{i,i} \frac{D^i}{\epsilon_{r_i}} + \sum_{p=1}^{8} \tilde{g}_{i,p} \frac{D^p}{\sqrt{\epsilon_{r_i}\epsilon_{r_p}}} \tag{26}$$

where

$$\tilde{g}_{i,p} = \tfrac{1}{4} \vec{A}_i \cdot \vec{A}_p$$

and the index p scans through the eight adjacent faces with contravariant flux's D^p and $\vec{A}_p$ is the contravariant vector of the pth face. It is noted that the geometric averaging of the permittivity is also included as specified in (30). For example, the projection of the electric field onto the primary grid edge $\vec{A}_1$ is

$$\begin{aligned} E_1|_{i,j,k}^{n+(1/2)} &= \vec{A}_1|_{i,j,k} \cdot \vec{A}_1|_{i,j,k} \frac{1}{\epsilon_{r|_{i,j,k}}} D^1|_{i,j,k}^{n+(1/2)} \\ &+ \frac{\vec{A}_1|_{i,j,k}}{4\sqrt{\epsilon_{r_{1|_{i,j,i}}}}} \cdot \left\{ \frac{\vec{A}_2|_{i,j,k}}{\sqrt{\epsilon_{r_{2|_{i,j,k}}}}} D^2|_{i,j,k}^{n+(1/2)} \right. \\ &+ \frac{\vec{A}_2|_{i+1,j,k}}{\sqrt{\epsilon_{r_{2|_{i+1,j,k}}}}} D^2|_{i+1,j,i}^{n+(1/2)} + \frac{\vec{A}_2|_{i,j-1,k}}{\sqrt{\epsilon_{r_{2|_{i,j-1,k}}}}} \\ &\cdot D^2|_{i,j-1,k}^{n+(1/2)} + \frac{\vec{A}_2|_{i+1,j-1,k}}{\sqrt{\epsilon_{r_{2|_{i+1,j-1,k}}}}} D^2|_{i+1,j-1,k}^{n+(1/2)} \\ &+ \frac{\vec{A}_3|_{i,j,k}}{\sqrt{\epsilon_{r_{3|_{i,j,k}}}}} D^3|_{i,j,k}^{n+(1/2)} + \frac{\vec{A}_3|_{i+1,j,k}}{\sqrt{\epsilon_{r_{3|_{i+1,j,k}}}}} \\ &\cdot D^3|_{i+1,j,k}^{n+(1/2)} + \frac{\vec{A}_3|_{i,j,k-1}}{\sqrt{\epsilon_{r_{3|_{i,j,k-1}}}}} D^3|_{i,j,k-1}^{n+(1/2)} \\ &+ \left. \frac{\vec{A}_3|_{i+1,j,k-1}}{\sqrt{\epsilon_{r_{3|_{i+1,j,k-1}}}}} D^3|_{i+1,j,k-1}^{n+(1/2)} \right\}. \end{aligned} \tag{27}$$

Each of the other projections are computed in this same straightforward manner. It is noted that the computational burden of this method is somewhat higher than the original formulation of Lee [3] since $G_{m,p}$ is unique for each of the nine field components which appear on the right-hand side of (27) and individual multiplications are required.

B. DSI/GY Algorithms

Similar to the NFDTD algorithm, DSI/GY algorithms are based on dual staggered grids. The principal difference is that DSI/GY algorithms are generalized to unstructured grids. To this end, the discrete electric and magnetic field intensity vectors are assumed to be parallel to each grid edge and constant along the length of the edge. A normal flux density vector is associated with each grid face. Again, Ampere's and Faraday's laws expressed in their integral form are enforced about each grid face. Approximating the time derivative of the flux results in an explicit update expression. Similar to the NFDTD algorithm, the normal flux vector must be projected onto the dual edge passing through its face. Due to the unstructured nature of the grid, this is done using a local field interpolation [4], [5], [9].

The face, which is uniquely shared by two cells unless it is on a Dirichlet or Neumann boundary, is assumed to be bound by N_{ej} edges that connect N_{ej} vertices. The kth vertex ($k = 1, N_{ej}$) of the jth face is shared by three faces of the lth cell ($l = 1$ or 2). Assume Faraday's law has been used to update the discrete normal magnetic flux densities. Then, the magnetic flux density associated with the kth vertex and the lth cell can be computed by solving the 3×3 system of equations

$$\begin{aligned} \vec{B}_{k,l} \cdot \hat{n}_j &= \vec{B} \cdot \hat{n}_j \\ \vec{B}_{k,l} \cdot \hat{n}_{k,l_1} &= \vec{B} \cdot \hat{n}_{k,l_1} \\ \vec{B}_{k,l} \cdot \hat{n}_{k,l_2} &= \vec{B} \cdot \hat{n}_{k,l_2} \end{aligned} \tag{28}$$

where $\hat{n}_{k,l_1}$ and $\hat{n}_{k,l_2}$ are unit vectors normal to each of the adjacent primary cell faces. Since the right-hand sides are all known after enforcing Faraday's law local to each face, (28) is used to solve for the three orthogonal components of $\vec{B}_{k,l}$. Subsequently, this is performed for each of the vertices of the face ($k = 1, N_{ej}$) and for each cell ($l = 1, 2$) shared by the face. Then, $\vec{B}_{k,l}$ is projected onto the dual edge with unit vector $\hat{s}_j$ along its length through a dot product, i.e., $\vec{B} \cdot \hat{s}_j$. The magnetic flux density vector over the face is then expressed by the interpolation of the local field values as

$$b_j = \frac{\sum_{l=1}^{2} \sum_{k=1}^{N_{ej}} |w_{k,l}| \vec{B}_{k,l} \cdot \hat{s}_j}{\sum_{l=1}^{2} \sum_{k=1}^{N_{ej}} |w_{k,l}|} \tag{29}$$

where $w_{k,l}$ are weighting factors to be determined. This equation then contributes to one row of A_b.

Employing some simple algebra, it can be shown from (28) that

$$\begin{aligned} \vec{B}_{k,l} \cdot \hat{s}_j = \frac{\hat{s}_j \cdot (\hat{n}_{k,l_1} \times \hat{n}_{k,l_2})}{\hat{n}_j \cdot (\hat{n}_{k,l_1} \times \hat{n}_{k,l_2})} \vec{B} \cdot \hat{n}_j + \frac{\hat{s}_j \cdot (\hat{n}_{k,l_2} \times \hat{n}_j)}{\hat{n}_j \cdot (\hat{n}_{k,l_1} \times \hat{n}_{k,l_2})} \\ \cdot \vec{B} \cdot \hat{n}_{k,l_1} + \frac{\hat{s}_j \cdot (\hat{n}_j \times \hat{n}_{k,l_1})}{\hat{n}_j \cdot (\hat{n}_{k,l_1} \times \hat{n}_{k,l_2})} \vec{B} \cdot \hat{n}_{k,l_2}. \end{aligned} \tag{30}$$

This allows for a simple computation of the projection coefficients as well as further insight into the asymmetry of the projection scheme. Specifically, it is observed that the first term contributes to a diagonal entry of A_b and the second two terms contribute to off diagonal entries. Next, presuppose that one was projecting onto the edge $\hat{s}_{k,l_1}$ passing through the face with normal $\hat{n}_{k,l_1}$. When interpolating using (28) and (29), the same corner would be involved in the interpolation. Following (30), the off-diagonal term contributing to updating $\vec{B} \cdot \hat{s}_{k,l_1}$ due to the flux $\vec{B} \cdot \hat{n}_j$ is

$$\frac{\hat{s}_{k,l_1} \cdot (\hat{n}_{k,l_1} \times \hat{n}_{k,l_2})}{\hat{n}_j \cdot (\hat{n}_{k,l_1} \times \hat{n}_{k,l_2})} \vec{B} \cdot \hat{n}_j. \tag{31}$$

This is the reciprocal term of the second term on the right-hand side of (30). As expected, the two terms share the same denominator, which is the volume of the parallel piped bound by the three unit normal vectors. The numerators are the triple scalar products of the edge vector with the two adjacent normal vectors. An interesting observation is that

$$\begin{aligned} (\hat{n}_{k,l_1} \times \hat{n}_{k,l_2}) = \vec{p}_j; \quad (\hat{n}_{k,l_2} \times \hat{n}_j) = \vec{p}_{l,k_1}; \\ (\hat{n}_j \times \hat{n}_{k,l_1}) = \vec{p}_{l,k_2} \end{aligned} \tag{32}$$

where $\vec{p}$ are vectors parallel to the edges of the primary grid. If the mesh was truly reciprocal, then the primary and secondary grids would share the same curvilinear coordinates (i.e., $\hat{p}_j = \hat{s}_j$). This would lead to a symmetric system. However, for an unstructured and irregular grid, this will only be true for special discretizations.

The question is how can one then enforce symmetry in the projections without sacrificing accuracy. An effective means

that has been used is to average the off-diagonal terms of A_b and A_d. Or assuming

$$a'_{b_{i,j}} = \tfrac{1}{2}(a_{b_{i,j}} + a_{b_{j,i}}). \quad (33)$$

To investigate the mathematical significance of this averaging scheme, it is seen that the second term in (30) will be modified as

$$\frac{1}{2}\left(\frac{\hat{s}_j \cdot (\hat{n}_{k,l_2} \times \hat{n}_j)}{\hat{n}_j \cdot (\hat{n}_{k,l_1} \times \hat{n}_{k,l_2})} + \frac{\hat{s}_{k,l_1} \cdot (\hat{n}_{k,l_1} \times \hat{n}_{k,l_2})}{\hat{n}_j \cdot (\hat{n}_{k,l_1} \times \hat{n}_{k,l_2})}\right) = \frac{1}{2}\,\frac{1}{\hat{n}_j \cdot (\hat{n}_{k,l_1} \times \hat{n}_{k,l_2})}\,(\hat{s}_j \cdot \vec{p}_{k,l_1} + \hat{s}_{k,l_1} \cdot \vec{p}_j). \quad (34)$$

The third term in (30) is modified in a similar manner. In essence, this averages the projections between the two dual coordinate systems. If the grid is regular yet nonorthogonal, the averaged formulation reduces back to the original algorithm in (30) since $\hat{p}_j = \hat{s}_j$.

Finally, the weights $w_{k,l}$ in (29) need be addressed. In the original formulation, Madsen proposed to use the triple scalar product $w_{k,l} = \vec{N}_j \cdot (\vec{N}_{k,l_1} \times \vec{N}_{k,l_2})$, where the $\vec{N}$ are the normal area vectors (i.e., $\vec{N}_j = A_j \hat{n}_j$ and A_j is the primary cell face area) [4]. The $w_{k,l}$ are identical for the corner shared by the two projections. However, the sum of the weights will not be the same for an irregular grid leading to asymmetry. Through experimentation, it has been found that choosing $w_{k,l} = 1$ is a sufficient and accurate weighting for prism elements.

The projection matrix A_d can be made symmetric in an identical fashion based on the secondary cell.

The proposed symmetric projection schemes have been found to work very well with unstructured quadrilateral prism elements. This is verified in Section V. However, the proposed symmetric projection operators are not accurate when using more generalized elements such as tetrahedron. The problem is that with tetrahedral meshes the dual-edge vectors can become highly skewed relative to one another. Hence, averaging the projections as proposed in (34) introduces significant error. For such elements, a more appropriate scheme is yet to be developed.

C. Discussion

It must be noted at this point that posing A_b and A_d as symmetric matrices is *not* sufficient for stability. They must also be positive definite. It is difficult to prove that the symmetric projection operators defined in (27) and in (33) and (34) are positive definite for all meshes. In fact, they are not. However, through extensive numerical experimentation using quadrilateral prism elements and hexahedron, it has been found that the symmetric forms proposed for A_b and A_d are positive definite for many general meshes. When this appears to break down is when an interior angle of a grid cell becomes very small (near 0°) or highly oblique (near 180°), A_b and A_d can contain negative real eigenvalues. Reviewing the unitary basis introduced for the NFDTD algorithm, it is seen that if an interior angle of a cell tends to 0° (or 180°), the local coordinate system becomes singular since the cell volume tends to zero as two of the curvilinear coordinates nearly align. This is similar for the DSI/GY algorithm, for which the triple scalar product in the denominator of (34) will tend to zero. Hence, this leads to ill-conditionedness in the projection operators. In practice, it has been found through numerical experimentation cells with an interior angle of a cell face smaller than about 10° or greater than about 170° should be avoided. Such thin elements are more easily avoidable when discretizing with unstructured meshes as opposed to structured meshing.

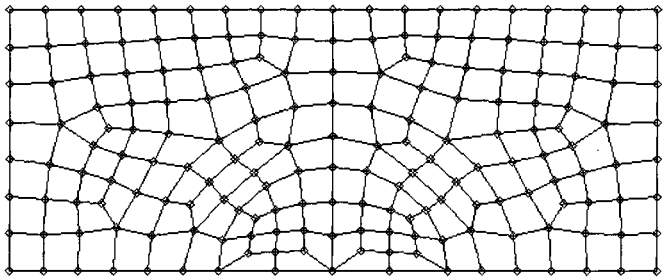

Fig. 1. Cross section of the small hexahedral mesh (primary grid) used for the eigenvalue analysis.

V. Validation

In this section, the proposed techniques are validated through numerical examples. All of the problems employ quadrilateral prism elements for both the DSI/GY and the simulations. These elements are orthogonal in the vertical direction and irregular quadrilaterals in the horizontal plane that are either unstructured (DSI/GY) or structured (NFDTD). Initially, a simple problem is presented for which an eigenvalue analysis of the explicit operators is performed. Then some deterministic solutions are presented to illustrate stability and accuracy of the methods.

A. Eigenvalue Analysis

To demonstrate the affect of the eigenspectrum on stability, an eigenvalue analysis of a simple problem is presented. To this end, an irregular and unstructured grid was generated to model a homogeneous cavity. A cross section of the grid is illustrated in Fig. 1. Only TM_z modes are excited by a vertical electric current source. Thus, it is sufficient to simulate the transverse magnetic fields and the vertical electric field. This was done to reduce the order of G, which will undergo a full eigenvalue analysis. The matrices C_e and C_h were constructed using the DSI/GY algorithm. A_b was constructed using (29) and (30), leading to an asymmetric sparse matrix. The projection matrix A_b was also constructed in a symmetric manner as outlined in (33) and (34). This symmetric matrix is referred to as A_b^s. Note that for this example A_d is an identity matrix since the TE fields were assumed to be zero.

The matrices $M = C_h A_b C_e$ and $M^s = C_h A_b^s C_e$ were explicitly constructed and the eigenvalues were computed using a numerical eigenvalue routine. The set of eigenvalues for M contained three complex conjugate pairs. This implies that this system is unstable. The eigenvalues of M^s were all real and > 0.

The matrix G was constructed using A_b and G^s was constructed using A_b^s. For both cases, $\Delta t = 0.9\tau$ was assumed, where τ is defined in (18). A plot of the eigenvalues of G and G^s in the right half of the complex plane is illustrated in Fig. 2. As a consequence of the properties of M, six conjugate pairs

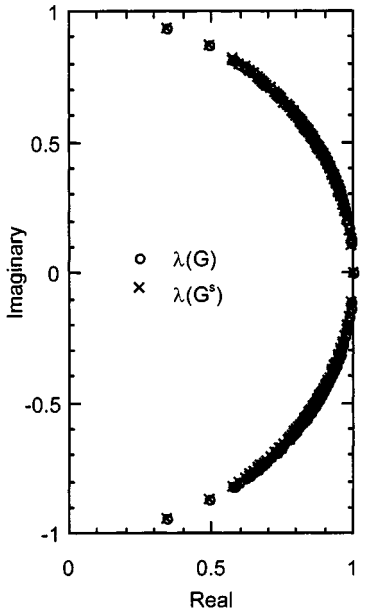

Fig. 2. Eigenvalues of G and G^s plotted in the complex plane.

of eigenvalues of G are off the unit circle. These eigenvalues are listed in Table I. Three of the pairs lie inside of the unit circle and three pairs lie *outside* the unit circle. Because these eigenvalues lie outside of the unit circle this system will ultimately be unstable. In fact, for this small example, the nonsymmetric case goes unstable after about 8000 time steps. As described in the Appendix, the instability occurred as a high-frequency oscillation, which grew exponentially in the late time. On the other hand, G^s was stable for over 250 000 time steps and showed no signs of impending instability. It is noted for the nonsymmetric case, that even as the time step was made smaller and smaller these spurious eigenvalues drifted closer to the unit circle but always remained outside of the unit circle. Conductive loss was also added into the domain. Even as the conductivity was dramatically increased, the nonsymmetric case had eigenvalues outside of the unit circle and was unstable in the late time.

B. Cavity Resonance Problem

A second example is now presented to study the accuracy of the symmetric projection operators. To this end, a benchmark test case of a circular dielectric ring in a rectangular PEC cavity is studied [12]. The geometry is provided in Fig. 3. Both unstructured and structured grids composed of quadrilateral prisms were generated to analyze this problem using the DSI/GY and NFDTD algorithms, respectively. A two-dimensional cross section of these grids are illustrated in Fig. 4.

The fields in the resonant cavity were simulated using the original NFDTD algorithm and G^{sym} presented in Section IV as well as the original DSI/GY algorithm and the symmetric projection algorithm presented in Section IV. The fields in the cavity were driven by injecting a vertically oriented current density placed at a nonsymmetric point described by

$$\vec{J}(t) = -\hat{z}\frac{2(t-t_o)}{t_w}e^{-((t-t_o)^2/t_w^2)} \tag{35}$$

TABLE I
EIGEVALUE PAIRS OFF THE UNIT CIRCLE OF G

$\lambda(G)$	$\lvert\lambda(G)\rvert$	$\angle\lambda(G)\rvert$
0.81936339±j0.57362192	1.00019921	±34.99519°
0.81903702±j0.57339344	0.99980096	±34.99519°
0.88046815±j0.47307256	0.99951078	±28.248988°
0.88133026±j0.47353577	1.00049152	±28.248988°
0.87688073±j0.48211204	1.00067569	±28.802146°
0.87569694±j0.48146119	0.99932478	±28.802146°

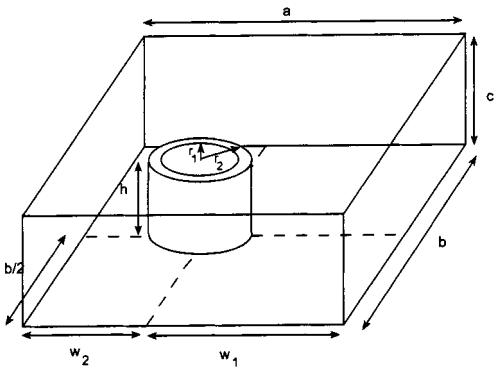

Fig. 3. Dielectric ring in a rectangular PEC cavity ($a = 324$ mm, $b = 121$ mm, $c = 43$ mm. The ring is centered at $w_1 = 207.25$ mm, $w_2 = 116.75$ mm, $b/2$ along the y-direction and rests on the ground plane. The ring has a height of $h = 39$ mm, inner radius $r_1 = 16.65$ mm, and outer radius ($r_2 = 26.75$ mm.)

where $t_w = 0.2122$ ns and $t_o = 3t_w$. The vertical field was probed in the cavity and the time simulation was performed for 25 000 time steps with $\Delta t = 4.5$ ps. The vertical field was Fourier transformed using an FFT and the resonant frequencies were extracted. Table II presents the resonant frequencies for the first four modes as calculated using the symmetric DSI/GY and NFDTD methods and the measured dominant mode [12]. These results are also compared to those obtained using an implicit FETD method [13] and the nonsymmetric algorithms. The resonant frequencies compare to within 0.1%. It is noted that for this case, the nonsymmetric DSI/GY method ran for 30 000 time steps before going unstable. The symmetric DSI/GY and NFDTD methods ran for 250 000 time steps and still showed no signs of instability.

The dielectric ring in cavity problem was repeated when the dielectric relative permittivity was increased to 9.8. For this case, the grid density in and near the ring was roughly doubled to properly resolve the fields. The calculated resonant frequencies are presented in Table III. Again, the symmetric DSI/GY simulation was stable for over 250 000 time steps. Interestingly, the symmetric NFDTD simulation did eventually go unstable in the very late time for this geometry. Observing Fig. 4(a), at each of the four corners of near the outer boundary of the dielectric ring, a cell is observed with a highly obtuse interior angle. For the refined mesh used in this case, this interior angle became more obtuse leading to an ill-conditioned matrix as discussed in the previous section. This is a penalty of structured gridding.

C. Patch Antenna

Finally, the microstrip-coupled circular patch antenna illustrated in Fig. 5 was modeled using the DSI/GY algorithm.

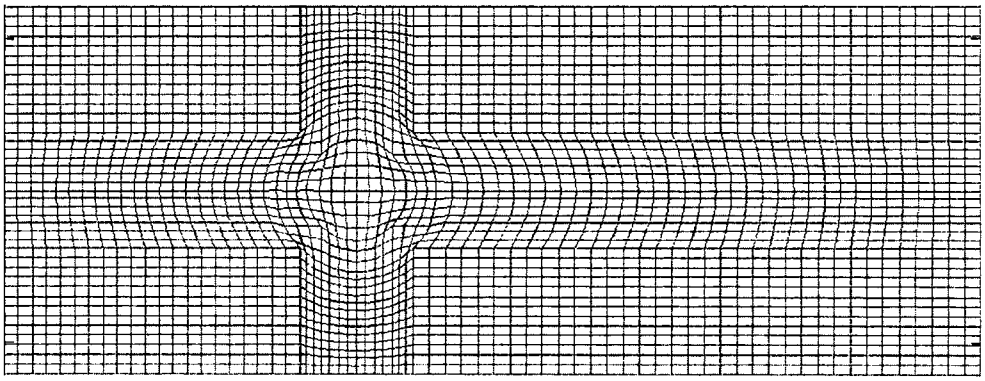

(a)

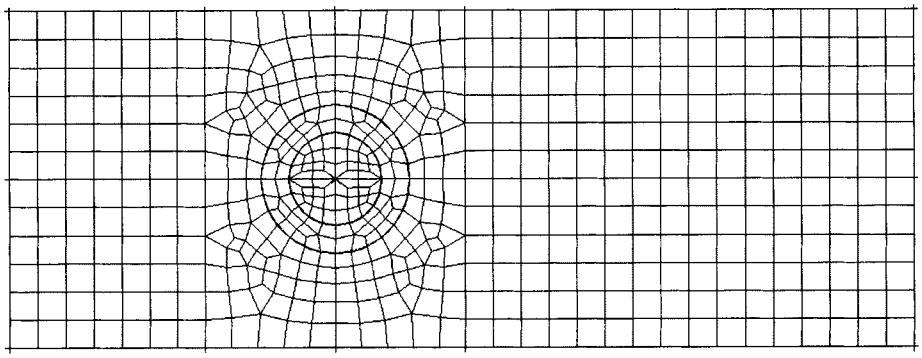

(b)

Fig. 4. Cross section of the mesh (primary grid) used to model the fields within the cavity. (a) Structured mesh. (b) Unstructured mesh.

TABLE II
RESONANT FREQUENCIES OF THE DIELECTRIC RING-LOADED CAVITY, ϵ_r = 2.06

Mode	Meas. [12]	WP-DSI	G^{sym}	FETD
k01	1.258 GHz	1.258 GHz	1.258 GHz	1.259 GHz
k02	-	1.509 GHz	1.509 GHz	1.512 GHz
k03	-	1.836 GHz	1.835 GHz	1.841 GHz
k04	-	2.158 GHz	2.161 GHz	2.175 GHz

TABLE III
RESONANT FREQUENCIES OF THE DIELECTRIC RING-LOADED CAVITY, ϵ_r = 9.8

Mode	WP-DSI	G^{sym}	FETD
k01	0.9520 GHz	0.9520 GHz	0.9518 GHz
k02	1.415 GHz	1.415 GHz	1.420 GHz
k03	1.608 GHz	1.612 GHz	1.615 GHz
k04	2.024 GHz	2.026 GHz	2.034 GHz

The patch antenna was also simulated using Zeland Software's IE3D, a commercial method of moments code [14], for a comparative solution. An unstructured mesh composed of quadrilateral prism elements was generated for the patch antenna that consisted of 159 600 hexahedron. The exterior boundaries of the mesh were terminated using an anisotropic perfectly matched layer (PML) [15] that was ten cells thick. The PML regions on the side walls and corner regions were composed of orthogonal cells. The top horizontal PML layer was composed of a mesh that is orthogonal along the vertical direction, but unstructured and nonorthogonal in the transverse direction (the exception is the corner regions where the mesh is orthogonal). Since the PML interface is planar, the interface is perfectly matched.

The GY simulation was performed using both the nonsymmetric formulation and the symmetric formulation outlined in Section IV. Both simulations were run for 20 000 time steps ($\Delta t = 0.725$ ps). The nonsymmetric formulation remained stable throughout the entire computation. However, ultimately it would go unstable. The magnitude of S_{11} as calculated using the GY code, the symmetric GY method, and the method of moment code (IE3D) is illustrated by the graph in Fig. 6. It is observed that enforcing symmetry in the projections introduces nearly negligible error to the computation. Both methods compare well with the method of moments solution with the exception of a slight shift in the resonant frequency.

VI. SUMMARY

In this paper, an analysis of the stability of generalized FDTD solutions has been presented. It was demonstrated that it is not sufficient to only restrict the time step for generalized grid FDTD schemes. Rather, numerical stability also requires that M be a positive definite matrix with real and distinct eigenvalues (where M is defined in (14)). This was demonstrated explicitly through a closed-form eigenvalue analysis.

For generalized grid schemes such as the NFDTD and DSI/GY algorithms, it was demonstrated that if the projection matrices are positive definite symmetric, then M will be positive definite. If the projection matrices are not positive

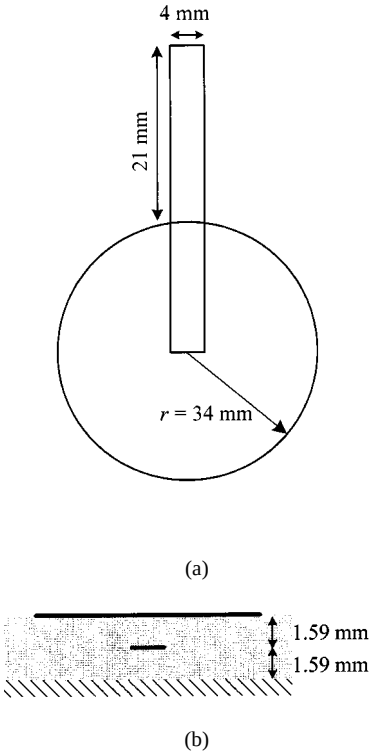

Fig. 5. Microstrip coupled circular patch antenna. The microstrip is printed on a 1.59-mm substrate ($\epsilon_r = 2.62$) over a ground plane and the patch antenna is printed above a 1.59-mm superstrate ($\epsilon_r = 2.62$). (a) Top view. (b) End view.

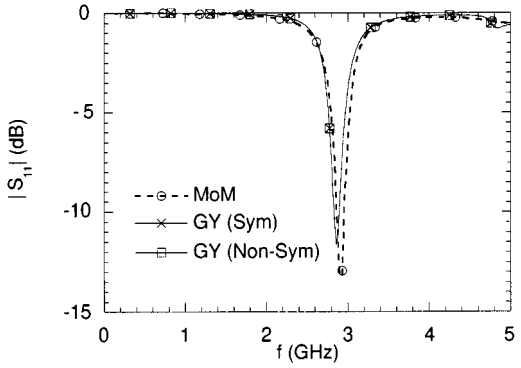

Fig. 6. Comparison of the reflection loss of the microstrip coupled circular patch antenna computed using the method of moments (MoM), the GY algorithm, and the symmetric GY algorithm.

definite symmetric the system is not numerically stable and will suffer from instabilities occurring in the late time and would be characterized by a high-frequency oscillation and an exponential growth in amplitude.

A scheme was introduced to construct symmetric projection matrices for the NFDTD and DSI/GY algorithms. While symmetry is not sufficient for stability, it was found that for quadrilateral prism elements, this scheme can result in positive definite symmetric projection matrices. However, it was found that if the mesh contains highly elongated or very narrow cells with interior angles breaching 0° or 180° the projection matrices will lose their positive definite properties. In general, automatic mesh generation schemes based on unstructured meshing will avoid such cells. However, for complex geometries, structured meshes upon which the NFDTD scheme is based may often contain such elements. For this reason, the DSI/GY algorithms tend to be more robust.

Through numerical validation, it was shown that the symmetric schemes provide stable and accurate results for quadrilateral prism elements. Unfortunately, these schemes are not applicable to meshes composed of general 3-D tetrahedral meshes for which alternate methods of imposing the projection operators are still under investigation.

The generalized FDTD equations presented by (1) and (2) are quite general and the eigenvalue analysis presented can be applied to the stability analysis of other FDTD-based schemes.

APPENDIX

Further insight into the characteristics of late-time instabilities can be gained by analyzing the properties of the space-eigenvalue problem. Assume that a volume discretization is defined over a volume Ω bound by a surface Λ. Then (1) and (2) are expressed in discrete space and continuous time as

$$\frac{\partial}{\partial t}\tilde{d} = C_h A_b \tilde{b} \tag{A.1}$$

$$\frac{\partial}{\partial t}\tilde{b} = -C_e D_\epsilon A_d \tilde{d} \tag{A.2}$$

where $\tilde{d}$ and $\tilde{b}$ are discrete in space and continuous in time and the coefficients of the matrices arising from the spatial discretization over Ω are assumed to be constant in time. Then, differentiating (A.1) with respect with time and substituting in (A.2) leads to

$$\frac{\partial^2}{\partial t^2}\tilde{d} = -C_h A_b C_e D_\epsilon A_d \tilde{d} = -M\tilde{d}. \tag{A.3}$$

Define the initial conditions

$$\{\tilde{d}(\vec{r},0) = f(\vec{r}); \vec{r} \in \Omega\} \quad \left\{\frac{\partial}{\partial t}\vec{d}(\vec{r},t) = g(\vec{r}); \vec{r} \in \Omega, t = 0\right\}. \tag{A.4}$$

Also, for simplicity, a Dirichlet boundary condition is defined on Λ, i.e., $\{\tilde{d}(\vec{r},t) = 0; \vec{r} \in \Lambda, t \geq 0\}$. Based on these initial conditions and boundary conditions, (A.3) is solved. Again, it is assumed that M is diagonalizable as in (14), where P is the matrix containing the complete set of eigenvectors of M. Then $\tilde{d}$ can be described as a linear combination of the eigenvectors as

$$\tilde{d} = \sum_{i=1}^{N} \overline{d}_i(t) P^{(i)} \tag{A.5}$$

where $P^{(i)}$ is the ith eigenvector and $\overline{d}_i(t)$ is a time-dependent coefficient. Substituting (A.5) and (A.3) and then performing a similarity transform based on P leads to

$$\frac{\partial^2}{\partial t^2}\overline{d}_i = -\lambda_{m_i}\overline{d}_i. \tag{A.6}$$

This has the general solution

$$\tilde{d} = \sum_{i=1}^{N} \left(f_{o_i} \cos(\sqrt{\lambda_{m_i}} t) + \frac{g_{o_i}}{\sqrt{\lambda_{m_i}}} \sin(\sqrt{\lambda_{m_i}} t) \right) P^{(i)} \tag{A.7}$$

where f_{o_i} and g_{o_i} are discrete coefficient vectors based on the initial conditions in (A.4).

The system of ordinary differential equations will thus be well posed or stable if the λ_m are real and $\lambda_m \geq 0$. Obviously, if the λ_m are < 0, this will lead to an unbounded growth of the solution. Furthermore, if a λ_{m_i} is complex, an unbounded growth with time would result. Specifically, assume a conjugate pair for $\lambda_{m_i} = \omega_c^2 e^{\pm j\phi}$. Then, expanding the trigonometric functions using Euler's law will lead to exponential terms of the form

$$e^{j\sqrt{\lambda_{m_i}} t} = e^{j\omega_c \cos(\phi/2)t \mp \omega_c \sin(\phi/2)t}. \tag{A.8}$$

Typically, the imaginary part of λ_{m_i} is quite small, leading to a very small ϕ. Subsequently, an instability will occur in the late time and will be dominated by the largest value of ω_c. Hence, the instability is characterized by a very high-frequency oscillation in the fields that ultimately grows in magnitude exponentially in the late time.

Finally, from this analysis, it is seen that if M does not have distinct (or simple) eigenvalues, a term with linear time dependence needs to be included in (A.7) (note that eigenvalues of zero are considered to be simple eigenvalues). This, of course, can lead to unbounded solutions.

ACKNOWLEDGMENT

The authors would like to thank the anonymous reviewers for their insightful and constructive comments.

REFERENCES

[1] A. Taflove, *Computational Electrodynamics: The finite-difference time-domain method*. Boston, MA: Artech House, 1995.
[2] T. G. Jurgens, A. Taflove, K. R. Umashankar, and T. G. Moore, "Finite-difference time-domain modeling of curved surfaces," *IEEE Trans. Antennas Propagat.*, vol. 40, pp. 357–366, Apr. 1992.
[3] J.-F. Lee, R. Palendech, and R. Mittra, "Modeling three-dimensional discontinuities in waveguides using nonorothogonal FDTD algorithm," *IEEE Trans. Microwave Theory Tech.*, vol. 40, pp. 346–352, Feb. 1992.
[4] N. Madsen, "Divergence preserving discrete surface integral methods for Maxwell's equations using nonorthogonal unstructured grids," *J. Computat. Phys.*, vol. 119, pp. 34–45, 1995.
[5] S. Gedney, F. Lansing, and D. Rascoe, "A full-wave analysis of passive monolithic integrated circuit devices using a generalized Yee-algorithm," *IEEE Trans. Microwave Theory Tech.*, vol. 44, pp. 1393–1400, Aug. 1996.
[6] J. A. Roden, "Broadband electromagnetic analysis of complex structures with the finite-difference time-domain technique in general curvilinear coordinates," Ph.D., Dept. Elect. Eng., Univ. Kentucky, Lexington, KY, 1997.
[7] I. J. Craddock, C. J. Railton, and J. P. McGeehan, "Derivation and application of a passive equivalent circuit for the finite-difference time-domain algorithm," *IEEE Microwave Guided Wave Lett.*, vol. 6, pp. 40–42, Jan. 1996.
[8] N. Madsen, "Divergence preserving discrete surface integral methods for Maxwell's equations using nonorthogonal unstructured grids,", Tech. Rep. UCRL-JC-109787, LLNL, Feb. 1992.
[9] S. Gedney and F. Lansing, "Explicit time-domain solutions of Maxwell's equations using nonorthogonal and unstructured grids," in *Finite Difference Time Domain Methods for Electrodynamic Analyzes*, A. Taflove, Ed. New York: Artech House, 1995.
[10] J. F. Lee, R. Lee, and A. Cangellaris, "Time-domain finite-element methods," *IEEE Trans. Antennas Propagat.*, vol. 45, pp. 430–442, Mar. 1997.
[11] B. Gustafsson, H.-O. Kreiss, and J. Oliger, *Time-Dependent Problems and Difference Methods*. New York: Wiley, 1995.
[12] I. Bardi, O. Biro, K. Preis, and B. R. Vrisk K. R., "Nodal and edge element analysis of inhomoheneous loaded 3-D cavities," *IEEE Trans. Magn.*, vol. 28, pp. 1141–1145, Feb. 1992.
[13] S. Gedney and U. Navdariwala, "An unconditionally stable implicit finite-element time-domain solution of the vector wave equation," *IEEE Microwave Guided Wave Lett.*, vol. 5, pp. 332–334, Oct. 1995.
[14] Zeland Software, , Freemont, CA.
[15] S. D. Gedney, "An anisotropic perfectly matched layer absorbing media for the truncation of FDTD lattices," *IEEE Trans. Antennas Propagat.*, vol. 44, pp. 1630–1639, Dec. 1996.

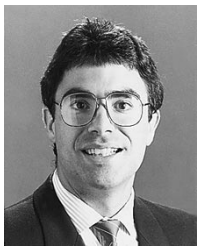

Stephen D. Gedney (S'84–M'91–SM'98) received the B.Eng. (honors) degree from McGill University, Montreal, P.Q., Canada, in 1985, and the M.S. and Ph.D. degrees in electrical engineering from the University of Illinois, Urbana-Champaign, in 1987 and 1991, respectively.

He is an Associate Professor of electrical engineering at the University of Kentucky, Lexington. From 1985 to 1987 he worked for the U.S. Army Corps of Engineers, Champaign, IL, where he was engaged in research in electromagnetic pulse simulation and propagation. Since 1991 he has been with the Department of Electrical Engineering, University of Kentucky. In the summers of 1992 and 1993 he was a NASA/ASEE Faculty Fellow at the Jet Propulsion Laboratory, Pasadena, CA. In 1996 he was a Visiting Professor at the Hughes Research Laboratories, Malibu, CA. His research specialty is computational electromagnetics.

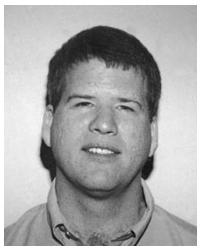

J. Alan Roden (M'90) received the B.S. degree from the University of Tennessee, Chattanooga, in 1984, the M.S. degree in electrical engineering from North Carolina State University, Raleigh, in 1988, and the Ph.D degree in electrical engineering from the University of Kentucky, Lexington, in 1997.

He is an Electromagnetic Compatibility (EMC) Design Engineer with the IBM Personal Systems Group, Research Triangle Park, NC. His industry experience includes positions in development and EMC engineering at the IBM Corporation, Research Triangle Park, NC. Previously, he worked with the Georgia Tech Research Institute, Atlanta, GA, where he was involved in applying numerical analysis techniques to scattering and radiation problems. He has coauthored a book chapter on nonorthogonal FDTD methods in *Advances in Computational Electrodynamics* (Boston, MA: Artech House, 1998) and has authored numerous technical works in related areas.